Intraband Mid-Infrared Transitions in Ag 2 Se Nanocrystals: Potential and Limitations for Hgfree Low Cost Photodetection

Junling Qu, Nicolas Goubet, Clément Livache, Bertille Martinez, Dylan Amelot, Charlie Gréboval, Audrey Chu, Julien Ramade, Hervé Cruguel, Sandrine Ithurria, et al.

Intraband Mid-Infrared Transitions in Ag_2Se Nanocrystals: Potential and Limitations for Hg-Free Low-Cost Photodetection

Junling Qu,[1] Nicolas Goubet,[1,2] Clément Livache,[1,2] Bertille Martinez,[1,2] Dylan Amelot,[2] Charlie Gréboval,[1] Audrey Chu,[1] Julien Ramade,[1] Hervé Cruguel,[1] Sandrine Ithurria,[2] Mathieu G. Silly,[3] Emmanuel Lhuillier[1*]

[1] Sorbonne Université, CNRS, Institut des NanoSciences de Paris, INSP, 4 place Jussieu, F-75005 Paris, France
[2]Laboratoire de Physique et d'Etude des Matériaux, ESPCI-Paris, PSL Research University, Sorbonne Université UPMC Univ Paris 06, CNRS, 10 rue Vauquelin 75005 Paris, France.
[3]Synchrotron-SOLEIL, Saint-Aubin, BP48, F91192 Gif-sur-Yvette Cedex, France

Abstract: Infrared photodetection based on colloidal nanoparticles is a promising path toward low cost devices. However, mid-infrared absorption relies on interband transitions in heavy metal-based materials, which is a major flaw for the development toward mass market. In the quest of mercury-free infrared active colloidal materials, we here investigate Ag_2Se nanoparticles presenting intraband transition between 3 and 15 µm. With photoemission and infrared spectroscopy, we are able to propose an electronic spectrum of the material in absolute energy scale. We also investigate the origin of doping and demonstrate that it results from a cation excess under Ag^+ form. We demonstrate photoconduction into this material under resonant excitation of the intraband transition. However, performances are currently quite weak with (i) a slow photoresponse (several seconds), and (ii) some electrochemical instabilities at room temperature.

To whom correspondence should be sent: el@insp.upmc.fr

INTRODUCTION

Thanks to the ease of color tunability from UV to THz range,[1] colloidal quantum dots (CQDs) have created extensive interest in applications such as displays and optoelectronics.[2,3] Their solution processability makes CQD-based infrared optoelectronics of utmost interest for the design of a new generation of low cost devices. In particular, CQD-based mid-infrared (IR) photodetection[4] has reached a high level of maturity with the demonstration of mid-IR photoconduction,[5] mid-IR focal plane array,[6] single particle photodetection,[7] multi-color photodetection,[8,9] plasmon assisted photodetection,[10,11] gas sensing[12] and fire detection.[13]All these demonstrated applications currently remain led by mercury chalcogenides compounds (HgS,[14,15] HgSe,[16,17] HgTe[18]) which present both interband[19] and intraband[20,21,22] transitions in the mid-IR range. However, the presence of mercury is often seen as a fundamental flaw of this technology.

Narrow energy transitions in the mid-IR typically require materials with a significant number of bands, which generally comes with a large atomic number and is thus heavy metal-free incompatible. The demand for non-toxic infrared active CQDs is more likely to result from doped semiconductors presenting intraband or plasmonic transitions. Several candidates might be considered such as extrinsically doped oxides, as Si nanocrystals and self-doped chalcogenides such as Ag_2Se. The latter material is of utmost interest in the sense that its surface chemistry is closer to those of the HgX compounds. Consequently the surface chemistry toolbox transfer to Ag_2Se materials seems more straightforward than to oxides or group IV compounds. Interest for Ag_2Se compounds was initially driven by near-IR photoluminescence[23,24] and thermoelectric applications.[25] Sahu *et al*[26,27] were the first to report mid-IR tunable transitions in Ag_2Se compounds; however, several questions are still unanswered, in particular the potential of this material for photoconduction and the exact nature of the mid-IR absorption feature. Recently, Park *et al*[28] answered to the latter question using spectroelectrochemistry and brought evidence of its intraband character. Here we expand the investigation on the Ag_2Se CQDs: we report about (i) the electronic structure of this material, (ii) the origin of doping in this material and finally (iii) the potential and the limitations of Ag_2Se CQDs for mid-IR photoconduction.

METHODS

Chemicals: Tri-n-octylphosphine oxide (TOPO, Alfa Aescar, 95%), Oleylamine (OLA, Acros, 80-90%), Trioctylphosphine (TOP, Cytek, 90%), Selenium powder (Strem Chemicals, 99.99%), Silver Chloride (AgCl, Alfa Aesar, 99.9%), Dodecanethiol (DDT, Sigma-Aldrich, 98%), 1,2,ethanedithiol (EDT, Fluka, 98.0%), Butanol (VMR, GPR RECTAPUR), Chloroform ($CHCl_3$, Carlo Erba), Ethanol absolute anhydrous (Carlo Erba, 99.9%), Lithium perchlorate ($LiClO_4$, Sigma-Aldrich, 98%) and Polyethylene glycol (PEG, M_w=6 kg/mol) were used.

Ag_2Se nanocrystal synthesis: 7.8 g of TOPO and 6.6 mL of OLA were put in a 50 mL three-neck flask. The mixture was degassed at 120 °C for 1 hour before the atmosphere was switched to argon. Then, 6 mL of selenium solution in TOP (1 M) was injected at 120 °C followed by heating the mixture to 140 °C, 180 °C or 250 °C. 4 mL of AgCl solution in TOP (1 M) was quickly injected at 140 °C and allowed to grow for 1 minute to obtain small-sized nanocrystals, injected at 180 °C and grew for 20 minutes to obtain large-sized ones, or injected at 250 °C for 20 minutes to obtain extra-large Ag_2Se nanocrystals. The growth reactions were quenched by 0.5 mL of DDT. After that, the flask was cooled down with air flux and 5 mL of butanol was injected at 60 °C to avoid the solidification of the reaction products. The nanocrystals were then precipitated with ethanol and redispersed with $CHCl_3$ twice. To obtain clean small-sized Ag_2Se, a 0.22 µm filter was also used after two washes.

FTIR: For infrared spectroscopy, we use a Vertex 70 from Bruker in the ATR configuration. The solution of nanocrystals is drop-casted on the diamond cell. Once the solvent is dried, the spectrum is acquired with a 4 cm^{-1} resolution and averaged 32 times.

TEM: For TEM pictures, a drop of diluted CQD solution is drop-casted onto a copper grid covered with an amorphous carbon film. A JEOL 2010F is used at 200 kV for the acquisition of pictures.

X-ray diffraction: X-ray diffraction is obtained by drop-casting the Ag_2Se CQD solution on a Si wafer. The diffractometer is a Philips X'Pert based on the emission of the Cu K_α line at λ=0.154 nm, operated at 40 kV and 40 mA.

EDX analysis: Energy dispersive X-ray (EDX) analysis is conducted by depositing a solution of nanocrystals onto Si wafer. The sample is then introduced into a FEI Magellan scanning electron microscope. The current of the beam is adjusted to 1.6 nA and the operating bias is set as 15 kV. The EDX analysis is obtained from an Oxford EDX probe.

RBS analysis: Rutherford Backscattering Spectrometry has been used as a complementary analysis to EDX to determine the Ag/Se ratio. To do so, the SAFIR source at INSP was used with He^+ as ion accelerated under 1.8 MeV. The beam size is 1.5 mm^2 and the collection angle is 165°. The He^+ beam current is operated at 50 nA. The energy calibration is done using a Bi-implanted Si wafer with a 6.10^{15} cm^{-2} dose. From the backscattered yield, the *Ag/Se ratio* is determined by $R = \frac{A_{Ag}}{A_{Se}}\left(\frac{Z_{Se}}{Z_{Ag}}\right)^2$ in which A_{Ag} denotes the area of the peak resulting from backscattering at Ag atoms, A_{Se} equals the area of the Se peak, and Z_{Ag} and Z_{Se} are the atomic number of Ag and Se, respectively.

Ultraviolet and X-ray photoemission measurements: For photoemission, the Ag_2Se nanocrystal solution has been drop-casted on an 80 nm gold coated Si/SiO_2 wafer. The film is then ligand exchanged using ethanedithiol as capping ligands. The ligand exchange is obtained by dipping the film into a solution of EDT (1%wt) in ethanol.

The valence band and the cut off of the secondary electrons have been obtained while exciting the film using a He lamp operated at 21.2 eV on the Tempo beamline of synchrotron Soleil, while for the core level the synchrotron beam operated at 600 eV has been used as X-ray photon source. The photoelectrons were detected at normal emission and at 46° from the polarization vector $\vec{E}$. The Fermi edge of a bulk gold substrate is used as energy reference (*ie* its binding energy is taken equal to 0 eV). All other spectra are shifted accordingly.

Si/SiO_2/Au electrodes: The surface of a Si/SiO_2 wafer (400 nm oxide layer) is cleaned by sonication in acetone. The wafer is rinsed with isopropanol and finally cleaned using an O_2 plasma. AZ 5214E resist is spin-coated and baked at 110 °C for 90 s. The substrate is exposed under UV through a pattern mask for 2 s. The film is further baked at 125 °C for 2 min to invert the resist. Then a 40 s flood exposure is performed. The resist is developed using a bath of AZ 726 for 32 s, before being rinsed in pure water. We then deposit a 5 nm chromium layer and 80 nm gold layer using a thermal evaporator. The lift-off is performed by dipping the film in acetone for 1 h. The electrodes are finally rinsed using isopropanol and dried by an air flow. The electrodes are 2.5 mm long and spaced by 10 µm. These electrodes are used for photoconductive device and electrolyte gated transistor measurements.

Electrolyte gating: For electrolyte gating we first mix in a glove box 0.5 g of $LiClO_4$ with 2.3 g of PEG. The vial is heated at 170 °C on a hot plate for 2 h until the solution becomes clear. To use the electrolyte, the solution is warmed around 100 °C and brushed on the top of the Ag_2Se CQD film.

Electrolyte gated field effect transistor measurements: To measure the transfer curve of the electrolyte gated transistor, the transistor is connected to a home-made probe station connected to a Keithley 2634B used as a sourcemeter. All measurements are conducted in air at room temperature and ambient pressure.

Photoconduction measurements: For photoconduction measurements with interband excitation at room temperature, we use a near infrared (1.55 µm) laser diode. The sample is connected to a Zurich instrument MFLI lock-in, which also biased the sample. The laser is mechanically chopped using a wheel and this signal is used as

reference by the lock-in. For low temperature measurements, the sample is introduced in a closed-cycle helium cryostat and cooled down. A quantum cascade laser operating at 4.4 µm is used to resonantly excite the intraband transition. The sample is biased using the source of Femto DLCPA-200 current amplifier, which is also used to magnify the current. The signal is acquired on a Tektronik TDS-5034 oscilloscope.

DISCUSSION

We first synthetize a series of Ag_2Se CQDs using the method proposed by Norris' group.[26,27] The quenching of the reaction has been updated by introducing some DDT at the end of the reaction to enhance colloidal stability and reduce the material aggregation. The infrared spectra for three sizes of Ag_2Se CQDs are given in Figure 1a. They are composed of an interband feature at short wavelength and a strongly absorbing peak in the mid-IR. Tuning the size of the nanoparticles (see Figure 1c and d and Figure S1) from 5 nm to 28 nm allows to tune the energy of the intraband feature from 2100 cm^{-1} (260 meV or 4.8 µm) to 650 cm^{-1} (80 meV or 15.4 µm). The synthesis leads to low size polydispersity, between 5 and 10 %. The lattice structure is particularly well resolved in the case of the large Ag_2Se CQDs, see Figure 1d, where the X-ray diffraction confirms a tetragonal structure (Figure 1b). In the following we will focus on the Ag_2Se small size CQDs because they present the best optical features to target photodetection in the 3-5 µm range.

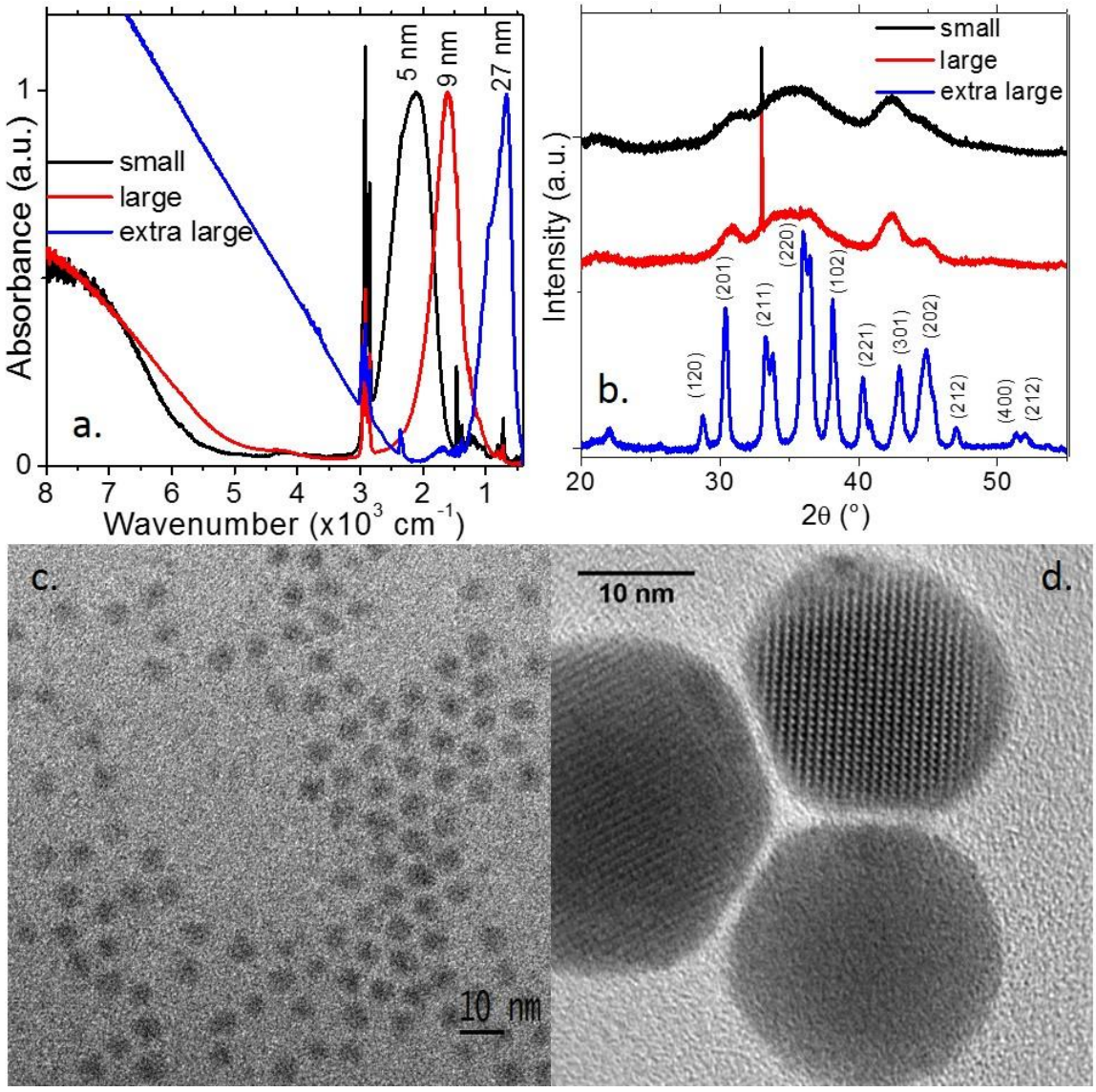

Figure 1a. Infrared spectra of films made of Ag_2Se CQDs with three different sizes. b. X-ray diffractogram of Ag_2Se CQDs with three different sizes. c. TEM image of small Ag_2Se CQDs. d. High resolution TEM image of extra large Ag_2Se CQDs.

The first open question is the electronic structure of the material in absolute energy scale, which is a critical step for the integration of this material into device with optimized ohmic contacts. To answer this question, we have conducted ultraviolet photoemission on Tempo beamline of Soleil Synchrotron. As shown in Figure 2a, a zoom on the cut-off of the secondary electrons reveals that the work function is equal to 4.3 eV. The low binding part of the spectrum (Figure 2b) is used to locate the valence band with respect to the Fermi energy and we deduce a value of V_b-E_f of 0.68 eV. Park et al[28], have deduced from spectroelectrochemistry the value of the interband gap to be 0.6 eV for this size of Ag_2Se CQD, which basically brings the $1S_e$ state of the conduction band below the Fermi level and confirms the degenerately *n*-doped nature of the Ag_2Se CQDs. From the energy of the intraband feature deduced from the IR spectrum, the $1P_e$ state is 260 meV above the $1S_e$ state. A reconstructed electronic spectrum is proposed in Figure 2c. In this sense, the obtained spectrum is quite close to the one previously observed for HgSe QDs with same sizes.[29]

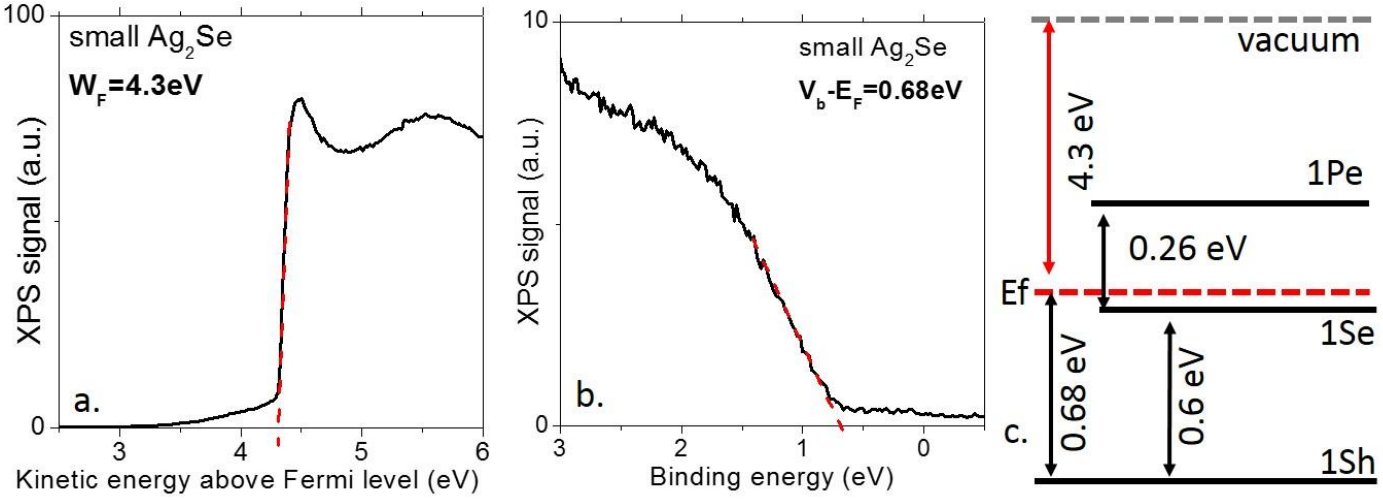

Figure 2a. X-ray photoemission signal around the cut off of the secondary electrons for a film made of small Ag_2Se CQDs. The determined work function is 4.3 eV. b. X-ray photoemission signal associated to the valence band for a film made of small Ag_2Se CQDs. c. Electronic spectrum in absolute energy scale from a film made of small Ag_2Se CQDs.

The origin of doping needs to be further investigated. Park *et al*[28] have reported a metal excess in these particles using Energy Dispersive X-ray spectroscopy (EDX). The actual stoichiometry of their compound is $Ag_{2.3}Se$. In our case EDX and Rutherford back scattering spectroscopy (RBS) gives consistent results of a silver excess and a final stoichiometry of $Ag_{2.6}Se$, see Figure S2 and S3. We attribute the fact to have even more silver than Park *et al* to the difference of synthetic process to grow the Ag_2Se CQDs. In II-VI semiconductor based CQDs, it is well known that surface tends to be metal rich leading to a n-type character.

The presence of metal silver is also further revealed by high-resolution transmission electron microscopy, see Figure 34 and S5. We indeed observe the presence of Janus nanoparticles, see Figure S4 with some darker spot on the QD image. A careful analysis of the diffraction pattern (Figure S4b-d) reveals that the main part of the particle is made of tetragonal Ag_2Se, while the dark spot is made of pure metallic silver. In addition, see figure S5, we also notice the presence of nanoparticles with a 5-fold symmetry which is characteristic of noble metal nanoparticles in face-centered cubic (fcc) lattice.[30,31,32] Thus, a naive explanation of doping may have been an energy transfer from the metallic Ag^0 phase to the narrow band gap semiconductor phase. Indeed Ag^0, thanks to its low work function is commonly used as electron injector for light emitting diode. However, this hypothesis is ruled out by X ray photoemission, which is the most suited tool to discriminate between two oxidation states of a chemical species, see Figure 3. The overview signal (Figure 3a) reveals the presence of gold from the substrate and oxygen due to air exposure of the sample while other peaks (Ag, Se for the semiconductor and S, C from the ligands) actually relate to the sample itself. The signal from the Ag 3d peak is shown in Figure 3b and without ambiguity can be fitted by a single Voigt contribution. The binding energy of the Ag $3d_{5/2}$ state is measured to be 368.06 eV, while the spin-orbit

coupling is 6 eV[33] and the full width at half maximum (FWHM) is 0.65 eV. This value of the binding energy is typically 200 meV below the value usually reported for Ag^0.[34] Moreover, no loss feature is observed in this spectrum which could have been a signature of metallic silver. Thus, we can confidently state that XPS only reveals Ag^+ and that the small Ag^0 island observed in TEM are just non-statistically representative of the sample. We can conclude that doping in Ag_2Se is somehow quite similar to most II-VI compounds for which the cation surface excess leads to a n-type character.[35,29] For the sake of completeness, we also have analyzed the signal relative to the Se 3d state, see Figure 3c. In this case, two components are observed, the most electron-rich peak is centered at a binding energy of 53.7 eV while the second peak presents a binding energy of 54.3 eV. Both contributions are fitted with a FWHM of 0.71 eV and spin orbit coupling of 0.86 eV.[33]

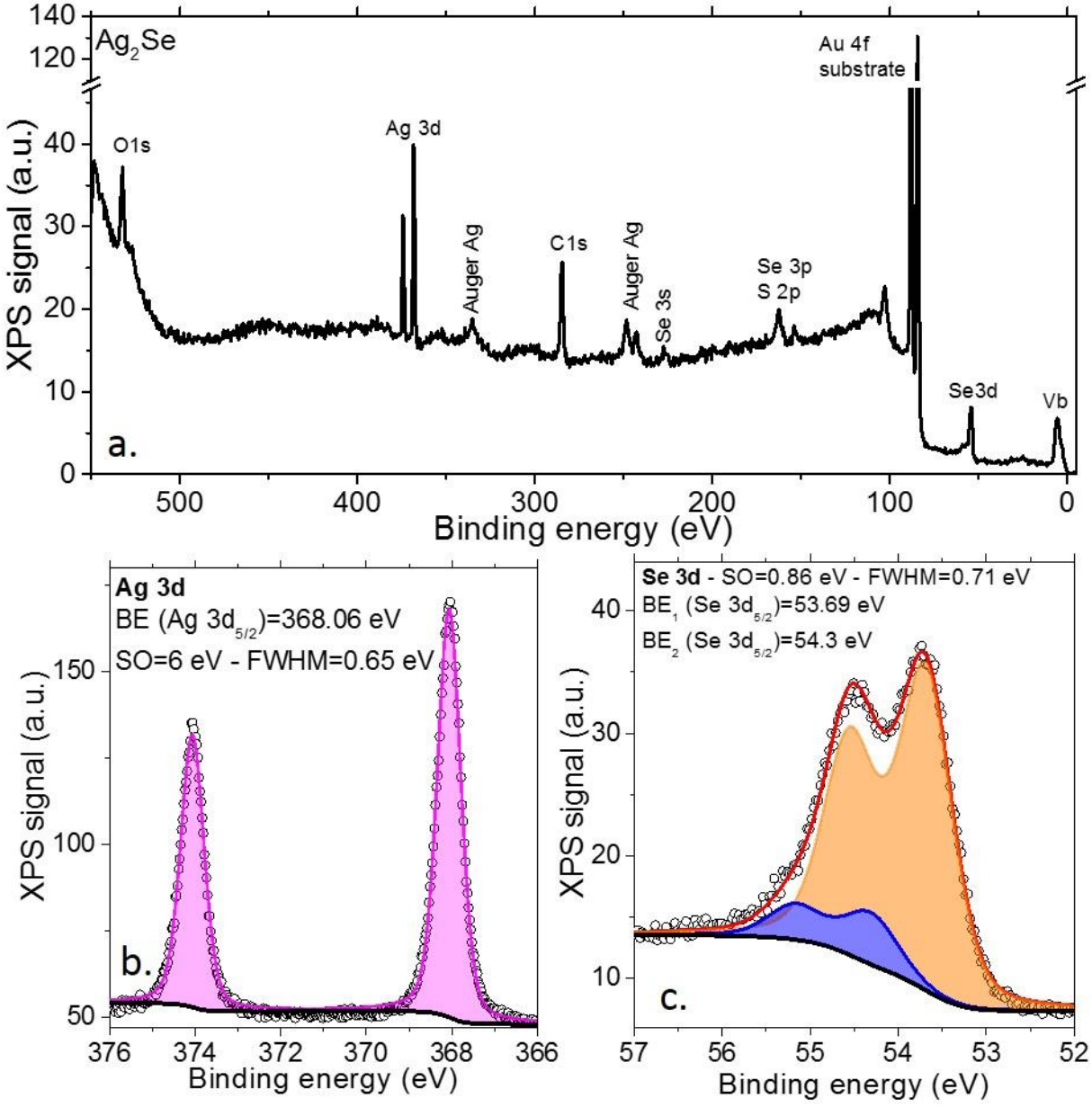

Figure 3a. X-ray photoemission overview of a film of Ag_2Se small nanoparticles deposited on a gold substrate. The photon energy is set to be 600 eV. b. X-ray photoemission signal relative to the Ag 3d state from a film of Ag_2Se small nanoparticles. c. X-ray photoemission signal relative to the Se 3d state from a film of Ag_2Se small nanoparticles.

In the following, we investigate the conduction and photoconduction properties of thin films made of Ag_2Se. At first, we integrate the small Ag_2Se CQDs into an electrolyte gated transistor[36] (a scheme of the device is proposed in Figure 4a). The latter is very convenient to tune the carrier density of heavily doped CQDs. To make the film of Ag_2Se CQDs conductive, we performed a solid-state ligand exchange toward EDT capping and check that this procedure

preserves the intraband feature (see Figure S6). The transfer curve (Figure 4b) reveals a clear n-type behavior with an increase of conductance upon electron injection (*ie* toward positive gate bias), which is fully consistent with the electronic spectrum proposed in Figure 2c. The on-off ratio of the transistor is typically around 50. In the following we have used two light sources to excite the small Ag_2Se CQDs: (*i*) a near infrared laser diode source at 1.55 µm to pump the interband transition and (*ii*) a quantum cascade laser source at 4.4 µm to resonantly excite the intraband transition. At room temperature and under near-IR illumination, the material presents a clear photoconductive behavior, see Figure 4c-e. The photocurrent presents a sub-linear dependence with the incident photon flux, see Figure 4c. The time response, see Figure 4d-e and S7, is for near -infrared excitation reasonably fast with a 3 dB cut-off frequency around 20 kHz. This behavior is obtained while the material is operated in the ohmic regime of the IV curve (*ie* below 200 mV). On the other hand, when the bias range is increased, the I-V curve starts to strongly deviate from linear regime and a clear electrochemical signature is observed, see Figure 4f. We speculate that the electrochemical behavior observed results from the limited stability of the Ag^+ oxidation state.

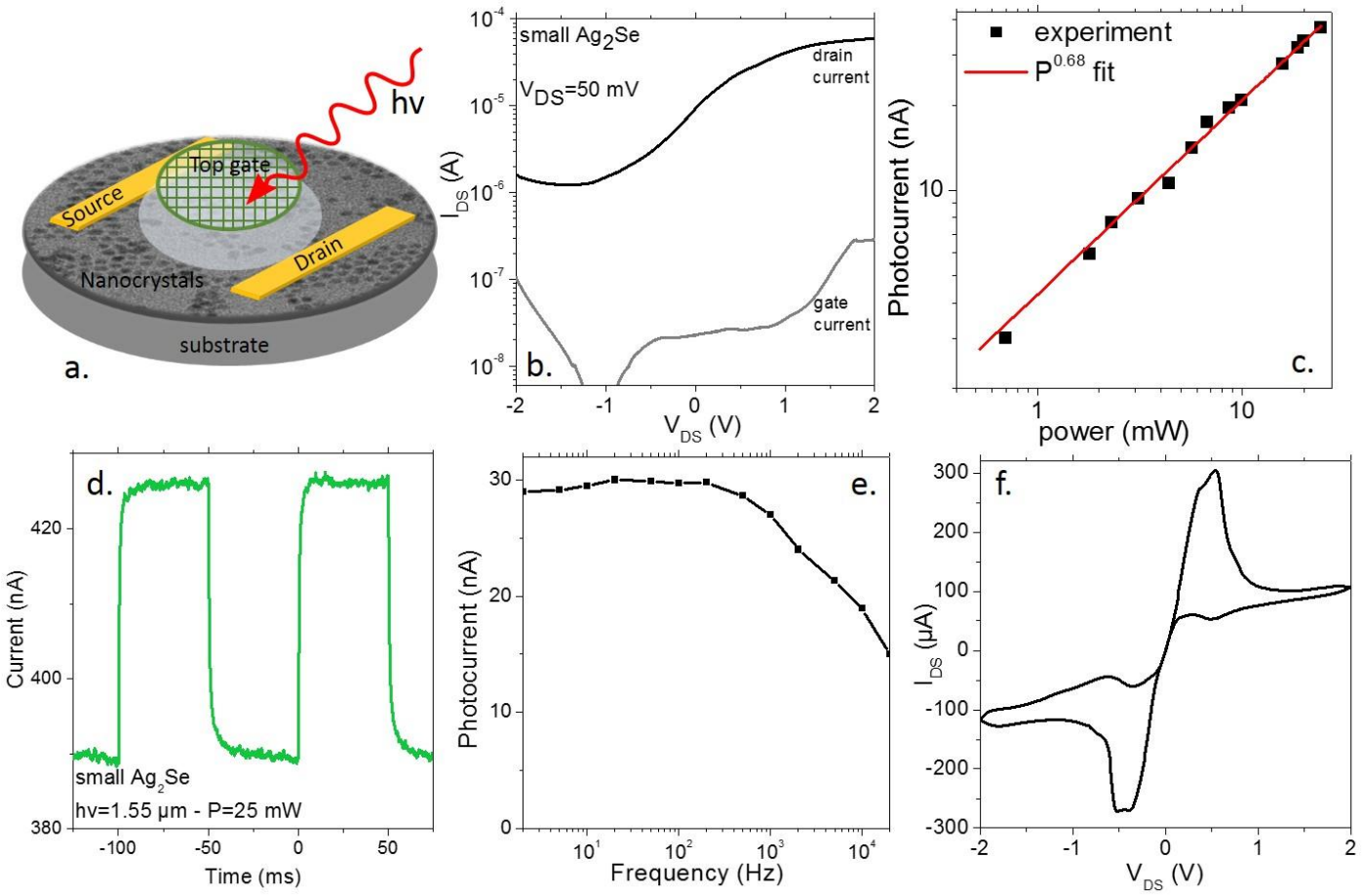

Figure 4a. Scheme of an electrolyte gated transistor for which the channel is made of a small Ag_2Se CQD film. b Transfer curve (drain current as a function of applied gate bias) for a film made of small Ag_2Se CQDs. c. Photocurrent as a function of the incident light power from a near-IR (λ=1.55 µm) laser diode. d. Time trace of the photocurrent while the near-IR laser is turned on and off. The laser power is set at 25 mW. e. Bode diagram (photocurrent as a function of signal frequency) for a film made of small Ag_2Se CQDs under illumination by the near-IR laser diode. f. IV curve of a film made of small Ag_2Se CQDs obtained when a larger range of biases is explored.

This electrochemical instability of the thin film of Ag_2Se CQDs is a severe limitation. We nevertheless observe that at low temperature, the material recovers its ohmic behavior, see figure S8, with no hysteresis. To finish, we explore the photoconductive behavior of the material at low temperature while we resonantly excite the intraband transition using quantum cascade laser as mid-IR source. A scheme of the experimental setup is given in Figure 5a. As the sample is cooled, the temperature dependence of the current follows a monotonic behavior, which can be fitted by an Arrhenius behavior. The activation energy in the 300 to 200 K range is 164 meV, see Figure 5b. This value

is within the accuracy of the photoemission experiment (50 meV) consistent with the energy spacing from the Fermi level to the $1P_e$ state (180 meV), which is the first empty state available for transport. To obtain a clear photocurrent signal while exciting the sample resonantly with the intraband absorption, very low temperature has to be reached (<200K), see Figure 5c-e and S9. The responsivity has been estimated to be 8 $\mu A.W^{-1}$, which is orders of magnitude lower than what has been reported for HgSe CQDs.[20,21] On the other hand, similarly to HgSe, the time response is extremely slow (several tens of s), see Figure 5d-e. This strongly contrasts with performance in HgTe CQDs where time response as short as 10 ns has been reported at the same wavelength.[37,38]

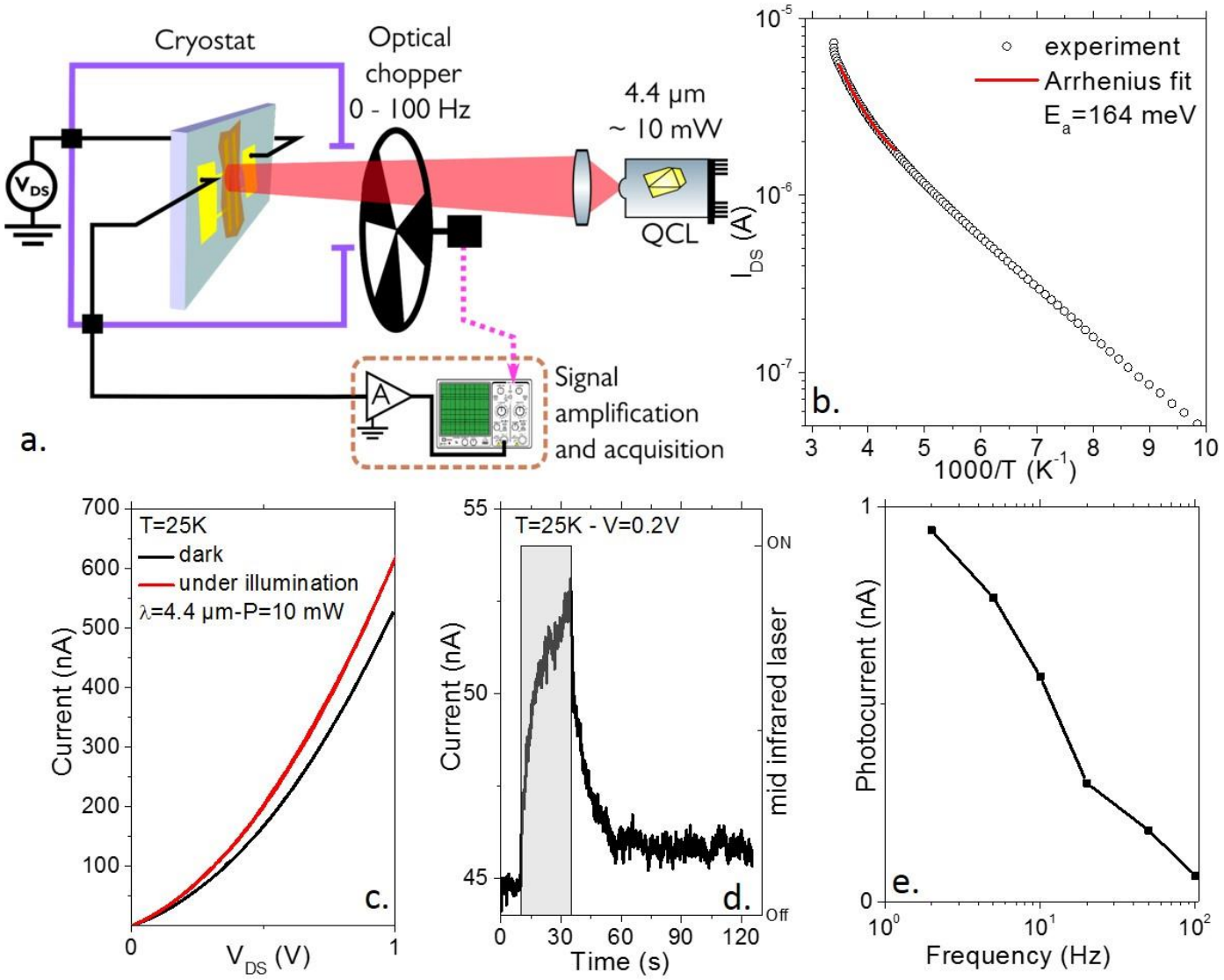

Figure 5 a. Scheme of the setup used for the illumination of the sample by a mid-IR source (ie a quantum cascade laser operated at 4.4 µm with a 10 mW power, Reprinted with permission from ref 38 (2018) American Chemical Society. b. Dark current under 1V as a function of the temperature for a film made of small Ag_2Se CQDs. c. IV curve for a film made of small Ag_2Se CQDs under dark condition and under illumination by the quantum cascade laser. d. Current as function of time while the mid-IR source is turned on and off. e. Bode diagram (photocurrent as a function of signal frequency) for a film made of small Ag_2Se CQDs.

CONCLUSION

We have explored the potential of Ag_2Se CQDs for mid-IR low-cost photoconduction as a heavy metal free colloidal material. Using photoemission and transport measurements, we have confirmed the degenerately n-type doping of the material and are able to propose an electronic spectrum in absolute energy scale where the work function is estimated to be 4.3 eV and the Fermi level is lying in the conduction band between the $1S_e$ and $1P_e$ state. A cation excess is observed from EDX and RBS analysis, in agreement with recent report on the same material[28] and the X-ray

photoemission demonstrates that the excess metal is under Ag^+ form. Thus doping is the result of material non-stoichiometry and the narrow band gap phase which makes possible the reduction of the particle by the environment as proposed for mercury chalcogenides compounds.[39] Material can be made photoconductive using conventional ligand exchange procedure, however we have observed a very limited range of bias stability (200 mV) likely due to oxidation and reduction of the Ag^+. This major failure needs to be solved, possibly by the addition of a shell, to really consider this material for room temperature IR photodetection. Under mid-IR excitation resonant with the intraband absorption, the photoconduction is determined to be very weak and slow compared to performances reported for Hg containing CQDs.

SUPPORTING INFORMATION

Supporting information includes additional structural (TEM), electronic (XPS, RBS, EDX) and transport measurements.

ACKNOWLEDEGMENTS

EL thanks the support ERC starting grant blackQD (grant number 756225). We acknowledge the use of clean-room facilities from the "Centrale de Proximité Paris-Centre". This work has been supported by the Region Ile-de-France in the framework of DIM Nano-K (grant dopQD). This work was supported by French state funds managed by the ANR within the Investissements d'Avenir programme under reference ANR-11-IDEX-0004-02, and more specifically within the framework of the Cluster of Excellence MATISSE and also by the grant Nanodose and H2DH. NG and AJ thank Nexdot for post doc funding.

REFERENCES

[1] Goubet, N.; Jagtap, A.; Livache, C.; Martinez, B.; Portalès, H.; Xu, X. Z.; Lobo, R.; Dubertret, B.; Lhuillier, E. Terahertz HgTe Nanocrystals: Beyond Confinement. *J. Am. Chem. Soc*. **2018**, *140*, 5033–5036.

[2] Konstantatos, G.; Sargent, E. H. Colloidal Quantum Dot Optoelectronics and Photovoltaics. Cambridge University Press, **2013**.

[3] Talapin, D. V.; Lee, J. S.; Kovalenko, M. V.; Shevchenko, E. V. Prospects of Colloidal Nanocrystals for Electronic and Optoelectronic Applications*. Chem. Rev.* **2010**, *110,* 389-458.

[4] Lhuillier, E.; Guyot-Sionnest, P. Recent Progresses in Mid Infrared Nanocrystal Based Optoelectronics. *IEEE J. Sel. Top. Quantum Electron.* **2017***, 23,* 1−8.

[5] Keuleyan, S.; Lhuillier, E.; Brajuskovic, V.; Guyot-Sionnest, P. Mid-infrared HgTe Colloidal Quantum Dot Photodetectors. *Nat. Photonics* **2011***, 5,* 489-493.

[6] Buurma, C.; Grein, C. H.; Guyot-Sionnest, P. MWIR Imaging with Low Cost Colloidal Quantum Dot Films, *Proc. SPIE 9933, Optical Sensing, Imaging, and Photon Counting: Nanostructured Devices and Applications*, **2016**, 993303.

[7] Wang, H.; Lhuillier, E.; Yu, Q.; Zimmers, A.; Dubertret, B.; Ulysse, C.; Aubin, H. Transport in a Single Self-Doped Nanocrystal. *ACS Nano* **2017**, *11*, 1222–1229.

[8] Lhuillier, E.; Robin, A.; Ithurria, S.; Aubin, H.; Dubertret, B. Electrolyte-Gated Colloidal Nanoplatelets-Based Phototransistor and its Use for Bicolor Detection. *Nano Lett.* **2014**, *14,* 2715-2719.

[9] Tang, X.; Tang, X.; Lai, K. W. C. Scalable Fabrication of Infrared Detectors with Multispectral Photoresponse Based on Patterned Colloidal Quantum Dot Films. *ACS Photonics* **2016**, *3*, 2396-2404.

[10] Chen, M.; Shao, L.; Kershaw, S. V.; Yu, H.; Wang, J.; Rogach, A. L.; Zhao, N. Photocurrent Enhancement of HgTe Quantum Dot Photodiodes by Plasmonic Gold Nanorod Structures. *ACS Nano* **2014**, *8*, 8208-8216.

[11] Yifat, Y.; Ackerman, M.; Guyot-Sionnest, P. Mid-IR Colloidal Quantum Dot Detectors Enhanced by Optical Nano-Antennas. *Appl. Phys. Lett.* **2017**, *110*, 41106.

[12] Chen, M.; Lu, H.; Abdelazim, N. M.; Zhu, Y.; Wang, Z.; Ren, W.; Kershaw, S. V.; Rogach, A. L.; Zhao, N. Mercury Telluride Quantum Dot based Phototransistor Enabling High Sensitivity Room-Temperature Photodetection at 2000 nm. *ACS Nano* **2017**, *11*, 5614–5622.

[13] Lacovo, A. D.; Venettacci, C.; Colace, L.; Scopa, L.; Foglia, S. High Responsivity Fire Detectors Based on Pbs Colloidal Quantum Dot Photoconductors. *IEEE Photonic TechL* **2017**, *29*, 703–706.

[14] Jeong, K. S.; Deng, Z.; Keuleyan, S.; Liu, H.; Guyot-Sionnest, P. Air-Stable n-Doped Colloidal HgS Quantum Dots. *J. Phys. Chem.Lett.* **2014**, *5*, 1139-1143.

[15] Kim, J.; Yoon, B.; Kim, J.; Choi, Y.; Kwon, Y. W.; Park, S. K.; Jeong, K. S. High Electron Mobility of β-HgS Colloidal Quantum Dots with Doubly Occupied Quantum States. *RSC Adv.* **2017**, *7*, 38166-38170.

[16] Sagar, L. K.; Walravens, W.; Maes, J.; Geiregat, P.; Hens, Z. HgSe/CdE (E=S,Se) Core/Shell Nanocrystals by Colloidal Atomic Layer Deposition. *J. Phys. Chem. C.* **2017**, *121*, 13816–13822.

[17]Jeong, J.; Yoon, B.; Kwon, Y. W.; Choi, D.; Jeong, K. S. Singly and Doubly Occupied Higher Quantum States in Nanocrystals. *Nano Lett.* **2017**, *17*, 1187-1193.

[18] Seong, H.; Cho, K.; Kim, S. Photocurrent Characteristics of Solution-Processed HgTe Nanoparticle Thin Films Under the Illumination of 1.3 μm Wavelength Light. *Semi. Sci. Tech.* **2008**, *23*, 075011.

[19] Kershaw, S. V.; Susha, A. S.; Rogach, A. L. Narrow Bandgap Colloidal Metal Chalcogenide Quantum dots: Synthetic Methods, Heterostructures, Assemblies, Electronic and Infrared Optical Properties. *Chem. Soc. Rev.* **2013**, *42*, 3033-3087.

[20] Zhiyou, D.; Kwang Seob, J.; Philippe, G. S. Colloidal Quantum Dots Intraband Photodetectors. *ACS Nano* **2014**, *8*, 11707-11714.

[21] Lhuillier, E.; Scarafagio, M.; Hease, P.; Nadal, B.; Aubin, H.; Xu, X. Z.; Lequeux, N.; Patriarche, G.; Ithurria, S.; Dubertret, B. Infrared Photodetection Based on Colloidal Quantum-Dot Films with High Mobility and Optical Absorption up to THz. *Nano Lett.* **2016**, *16*, 1282-1286.

[22] Jagtap, A.; Livache, C.; Martinez, B.; Qu, J.L.; Chu, A.; Gréboval, C.; Goubet, N.; Lhuillier, E. Emergence of Intraband Transitions in Colloidal Nanocrystals. *Opt. Mater. Express.* **2018**, *8,* 1174-1183.

[23] Gu, Y. P.; Cui, R.; Zhang, Z. L.; Xie, Z. X.; Pang, D. W. Ultrasmall Near-Infrared Ag_2Se Quantum Dots with Tunable Fluorescence for In Vivo Imaging. *J. Am. Chem. Soc.* **2012**, *134*, 79-82.

[24] Langevin, M. A.; Lachancequirion, D.; Ritcey, A. M.; Allen, C. N. Size-Dependent Extinction Coefficients and Transition Energies of Near-Infrared β-Ag_2Se Colloidal Quantum Dots. *J. Phys. Chem. C.* **2013**, *117*, 5424−5428.

[25] Yang, S.; Cho, K.; Park, Y.; Kim, S. Bendable Thermoelectric Generators Composed of p- and n-type Silver Chalcogenide Nanoparticle Thin Films. *Nano Energy.* **2018**, *49*, 333-337.

[26] Sahu, A.; Khare, A.; Deng, D. D.; Norris, D. J. Quantum Confinement in Silver Selenide Semiconductor Nanocrystals. *Chem Commun*. **2012**, *48*, 5458-5460.

[27] Sahu, A.; Qi, L.; Kang, M. S.; Deng, D.; Norris, D. J. Facile Synthesis of Silver Chalcogenide (Ag_2E; E=Se, S, Te) Semiconductor Nanocrystals. *J. Am. Chem. Soc.* **2011**, *133*, 6509–6512.

[28] Park, M.; Choi, D.; Choi, Y.; Shin, H.; Jeong, K.S. Mid-Infrared Intraband Transition of Metal Excess Colloidal Ag_2Se Nanocrystals. *ACS Photonics.* **2018,** 5, 1907-1911.

[29] Martinez, B.; Livache, C.; Mouafo, L. N.; Goubet, N.; Keuleyan, S.; Cruguel, H.; Ithurria, S.; Aubin, H.; Ouerghi, A.; Doudin, B.; *et al*, HgSe Self-Doped Nanocrystals as a Platform to Investigate the Effects of Vanishing Confinement. *ACS Appl. Mater. Interfaces.* **2017***, 9,* 36173−36180*.*

[30] Goubet, N.; Tempra, I.; Yang, J.; Soavi, G.; Polli, D.; Cerullo, G.; Pileni, M. P. Size and Nanocrystallinity Controlled Gold Nanocrystals: Synthesis, Electronic and Mechanical Properties. *Nanoscale* **2015**, *7*, 3237–3246.

[31] Ino, S.; Ogawa, S. Multiply Twinned Particles at Earlier Stages of Gold Film Formation on Alkalihalide Crystals. *Journal of the Physical Society of Japan* **1967**, *22*, 1365–1374.

[32] Goris, B.; De Beenhouwer, J.; De Backer, A.; Zanaga, D.; Batenburg, K. J.; Sánchez-Iglesias, A.; Liz-Marzán, L. M.; Van Aert, S.; Bals, S.; Sijbers, J.; *et al* Measuring Lattice Strain in Three Dimensions Through Electron Microscopy. *Nano Lett.* **2015**, *15*, 6996–7001.

[33] Wagner, C.D.; Rigges, W.M.; Davis, L.E.; Moulder J.F.; Muilenberg, G.E. Hanbook of X-ray Photoelectron Spectroscopy, Perkin Elmer, Eden Prairie, **1979.**

[34] Chen, Z.; Wang, W.; Zhang, Z.; Fang, X. High-Efficiency Visible-Light-Driven Ag_3PO_4/AgI Photocatalysts: Z-Scheme Photocatalytic Mechanism for their Enhanced Photocatalytic Activity. *J. Phys Chem C*. **2013**, *117*, 19346.

[35] Cruguel, H.; Livache, C.; Martinez, B.; Pedetti, S.; Pierruci, D.; Izquierdo, E.; Dufour, M.; Ithurria, S.; Aubin, H.; Ouerghi, A.; *et al*, Electronic Structure of CdSe-ZnS 2D Nanoplatelets. *Appl. Phys Lett.* **2017,** *110*, 152103.

[36] Lhuillier, E.; Ithurria, S.; Descamps Mandine, A.; Douillard, T.; Castaing, R.; Xu, X. Z.; Taberna, P. L.; Simon, P.; Aubin, H.; Dubertret, B. Investigating the n- and p-Type Electrolytic Charging of Colloidal Nanoplatelets. *J. Phys. Chem. C.* **2015***, 119,* 21795–21799.

[37] Martinez, B.; Livache, C.; Goubet, N.; Jagtap, A.; Cruguel, H.; Ouerghi, A.; Lacaze, E.; Silly, M. G.; Lhuillier, E. Probing Charge Carrier Dynamics to Unveil the Role of Surface Ligands in HgTe Narrow Band Gap Nanocrystals. *J. Phys. Chem. C.* **2018**, *122,* 859–865.

[38] Livache, C.; Goubet, N.; Martinez, B.; Jagtap, A.; Qu, J.; Ithurria, S.; Silly, M. G.; Dubertret, B.; Lhuillier, E. Band-Edge Dynamics and Multiexciton Generation in Narrow Band Gap HgTe Nanocrystals. *ACS Appl. Mater. Interfaces* **2018***, 10,* 11880–11887.

[39] Robin, A.; Livache, C.; Ithurria, S.; Lacaze, E.; Dubertret, B.; Lhuillier, E. Surface Control of Doping in Self-Doped Nanocrystals. *ACS Appl. Mat. Interface* **2016,** *8*, 27122−27128.

TOC graphic